Title

Rational Design of a Uranyl Metal–Organic Framework for the Capture and Colorimetric Detection of Organic Dyes

Journal

Chemistry - A European Journal, 26(61)

ISSN

0947-6539

Authors

Surbella, Robert G
Carter, Korey P
Lohrey, Trevor D
et al.

Publication Date

2020-11-02

DOI

10.1002/chem.201905766

Peer reviewed

Full Paper
doi.org/10.1002/chem.201905766

Photoluminescence

Rational Design of a Uranyl Metal–Organic Framework for the Capture and Colorimetric Detection of Organic Dyes

Robert G. Surbella III,*[a] Korey P. Carter,[b] Trevor D. Lohrey,[b, c] Dallas Reilly,[a] Mark Kalaj,[d] Bruce K. McNamara,[a] Jon Schwantes,[a] and Rebecca J. Abergel[b]

Abstract: A new uranyl containing metal–organic framework, **RPL-1**: $[(UO_2)_2(C_{28}H_{18}O_8)] \cdot H_2O$ (RPL for Radiochemical Processing Laboratory), was prepared, structurally characterized, and the solid-state photoluminescence properties explored. Single crystal X-ray diffraction data reveals the structure of **RPL-1** consists of two crystallographically unique three dimensional, interpenetrating nets with a 4,3-connected tbo topology. Each net contains large pores with an average width of 22.8 Å and is formed from monomeric, hexagonal bipyramidal uranyl nodes that are linked via 1,2,4,5-tetrakis(4-carboxyphenyl)benzene (TCPB) ligands. The thermal and photophysical properties of **RPL-1** were investigated using thermogravimetric analysis and absorbance, fluorescence, and lifetime spectroscopies. The material displays excellent thermal stability and temperature dependent uranyl and TCPB luminescence. The framework is stable in aqueous media and due to the large void space (constituting 76% of the unit cell by volume) can sequester organic dyes, the uptake of which induces a visible change to the color of the material.

Introduction

The study of actinide containing metal–organic frameworks (MOFs) has increased in recent years due to their propensity to form structurally diverse architectures and novel structure types that often exhibit unique chemical and physical properties.[1] Uranyl-containing frameworks garner much attention in this regard owing to their rich coordination chemistry and inherent luminescence properties, the latter having been explored for use in X-ray scintillation[2] and various visible and UV-light mediated processes, such as photocatalysis[3] and molecular sensing.[4] The crystal chemistry of uranyl-containing coordination polymers and frameworks is therefore well-developed, but despite this, the rational design of three-dimensional MOFs remains a challenge because of the linear nature of the uranyl cation.[5] The two axial oxo ligands (often) do not participate in additional bonding interactions and further ligand coordination is restricted to the equatorial plane. This planar coordination mode gives rise to square, pentagonal, and hexagonal bipyramidal building units that tend to assemble into 1- and 2D dimensional structure types.[6] There are several synthetic strategies for overcoming this geometric limitation and preparing uranyl materials with higher dimensionality, including 1) the incorporation of a secondary metal center as a 3D structure-directing agent or 2) using a non-planar, multitopic ligand to promote coordination outside of the equatorial plane of the uranyl cation.

Efforts to prepare heterometallic uranyl containing materials have given rise to a structurally diverse class of compounds[7] and provided a platform to promote and explore properties that may otherwise be inaccessible without contributions from both metal centers.[8] This synthetic approach has demonstrated great promise, yet is not aligned with our interest in exploring uranyl luminescence in MOFs free from the influence of a secondary metal center. For this reason, the alternative approach of using a non-planar ligand to induce the formation of a higher dimensional material was preferable. This synthetic strategy is discussed elsewhere[9] and as such, is only illustrated here by comparing the dimensionality of two different uranyl coordination polymers prepared from 1,3,5-tris(4-carboxyphenyl) benzene (TCB) and 5′-(4-carboxyphenyl)-2′,4′,6′-trimethyl[1,1′:3′,1″-terphenyl]-4,4″-dicarboxylic acid (TCB-$(CH_3)_3$), respectively (Figure 1). The three carboxylate groups in TCB are coplanar and thus, when combined with the uranyl cation yield a 2D network.[10] In contrast, the TCB$(CH_3)_3$ ligand is not planar due to the steric hindrance of the methyl groups (on the central benzene ring) and as a consequence, the carboxylate groups promote connectivity outside of the equatorial plane of the uranyl cation and give rise to a 3D architecture.[11] Tetradentate ligands have also proven exemplary in this regard as the carboxylate groups of 4,4′,4″,4‴-(pyrene-1,3,6,8-tetryl)-

[a] R. G. Surbella III, D. Reilly, B. K. McNamara, J. Schwantes
Pacific Northwest National Laboratory, Richland, Washington 99354 (USA)
E-mail: Robert.surbella@pnnl.gov

[b] K. P. Carter, T. D. Lohrey, R. J. Abergel
Chemical Sciences Division, Lawrence Berkeley National Laboratory
Berkeley, CA 94720 (USA)

[c] T. D. Lohrey
Department of Chemistry, University of California, Berkeley, CA 94720 (USA)

[d] M. Kalaj
Department of Chemistry and Biochemistry
University of California, San Diego, La Jolla, CA 92093 (USA)

Supporting information and the ORCID identification number(s) for the author(s) of this article can be found under:
https://doi.org/10.1002/chem.201905766.

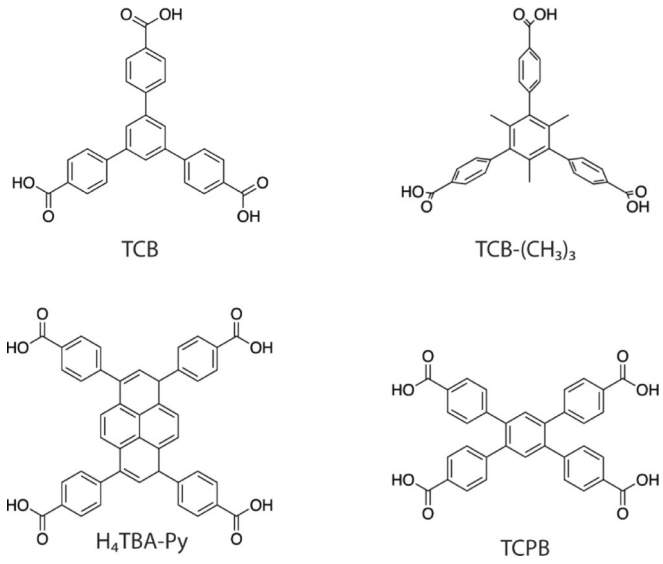

Figure 1. Multitopic ligands that have been used in the synthesis of multi-dimensional uranyl containing frameworks.

tetrabenzoic acid (H_4TBA-Py) and 1,2,4,5-tetrakis(4-carboxyphenyl)benzene (TCPB) for instance, are nearly perpendicular to the central benzene and are therefore suitable for preparing 3D MOFs with actinides, transition metals, and lanthanides.[12]

Here, we have chosen to pair TCPB with the uranyl cation in an effort to prepare a luminescent 3D MOF with permanent porosity. Recently, porous uranyl containing frameworks with high surface area have been investigated as possible adsorbent materials for the sequestration of radioisotopes[10] and organic dyes,[12c,13] the latter having widespread commercial and industrial utility, but adverse environmental consequences. The development of MOFs for the capture of harmful environmental toxins is of practical importance,[14] yet our interests are admittedly, more fundamental and focused on exploring analyte capture and/or exchange. To this end, we have chosen to study the adsorption of organic dye molecules to evaluate molecular adsorption. The utility and potential application of luminescent uranyl coordination compounds in general, is well-studied especially with respect to photocatalysis.[15] Despite this, luminescent uranyl containing MOFs that feature permanent porosity remain underexplored.[1f] It is therefore our long-term goal to develop a synthetic protocol for the preparation of luminescent 3D uranyl MOFs that may serve as a platform to explore molecular sequestration, sensing, or catalysis. Herein, we present the synthesis, crystallographic, and photophysical characterization of a novel uranyl containing MOF constructed from hexagonal bipyramidal uranyl building units and TCPB linkers.

Results and Discussion

The combination of TCPB and uranyl nitrate in *N*,*N*-dimethylformamide (DMF) at 100 °C for 24 hours led to the formation of **RPL-1**, $[(UO_2)_2(C_{28}H_{18}O_8)] \cdot H_2O$. Large yellow-green single crystals were harvested directly from the mother liquor and prepared for the X-ray diffraction experiment, whereas the pale yellow-green bulk material was washed three times with warm DMSO, followed by ethanol and water, dried, and isolated for analysis. Multiple attempts to collect high quality diffraction data using traditional laboratory X-ray sources (e.g., Ag, Cu, or Mo radiation generated from seal tubes and/or microfocus sources) were unsuccessful as the crystals diffracted extremely weakly. Data collection was attempted on numerous specimens and was suitable for only unit cell determination ($C2/c$; $a = 48.490(5)$ Å, $b = 46.089(6)$ Å, $c = 35.149(7)$ Å, $\beta = 133.175(3)^\circ$, $V = 57\,286.1$ Å^3). The single crystal X-ray diffraction capability at the Advanced Light Source at Lawrence Berkeley National Laboratory was needed to obtain diffraction data of sufficient quality for structure solution. Details of the diffraction experiment, additional synthetic notes (including comments regarding reproducibility and purity), and the spectroscopic data are located in the Supporting Information (Figures S1–8 and Tables S1 and 2).

The diffraction data reveals **RPL-1** consists of four crystallographically unique hexagonal bipyramidal uranyl building units that are each chelated by the carboxylate groups of three separate TCPB ligands to form 3D cages (Figure 2 and Figure 3). The cages are in turn linked by the TCPB ligands into two discrete, yet structurally identical 3D interpenetrating nets with tbo topology.[16] The nets are 4,3-connected and similar to those in related uranyl containing MOFs (e.g., NU-1300 and TCPP-U1).[12c,17] The connectivity is notable as 3,4-connected tbo type topologies are the norm in for example, the HKUST-1 series that features Cu paddlewheels and trimesic acid linkers.[18] Each net in **RPL-1** is porous and features channels that propagate along the [100], [010], [001], and [101] directions. The resulting solvent accessible void space constitutes 76% of the unit cell by volume or 43 343 Å^3 (which is 10 803 electrons per unit cell) (Figures S9–11). The accessible void space is likely much lower because the pores are obstructed by the interpenetration of the two nets. Brunauer–Emmett–Teller (BET) analysis is consistent with this crystallographic assessment as the experimentally determined surface area (measured by $N_{2(g)}$ adsorption) is only 9.6 m^2 g^{-1}, despite the experimentally determined average pore size being 22.8 Å wide (Figure S12 and Table S3). Save for a handful of water molecules, the majority of solvent molecules within the pores of **RPL-1** were unable to be modelled crystallographically and as such, the residual electron density in the pores was treated using SQUEEZE.[19] We found no evidence for the presence of ionic guest species and report the framework as charge neutral.

The thermal stability of **RPL-1** was assessed in $Ar_{(g)}$ and air (20% $O_{2(g)}$). The data reveal the material is stable until approximately 420 °C (Figure S13). Two distinct features that roughly sum to a 16% mass loss occur between 30 °C and 420 °C in the analysis performed in $Ar_{(g)}$. This is attributed to the loss of surface waters and solvent (e.g., water and DMF). The material completely degrades above 420 °C to a stable black soot. The data collected in air yields similar results. A 3% mass loss is observed between 30 °C and 125 °C and thereafter the material gradually decreases in mass (by roughly 11%) until ≈375 °C. Between 375 °C and 400 °C a second loss occurs that equates

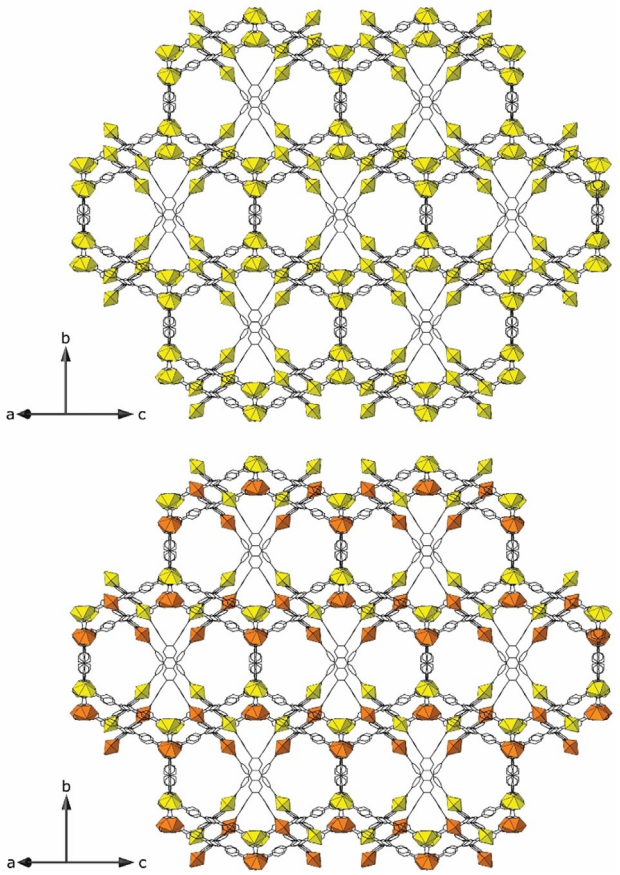

Figure 2. Top: The structure of **RPL-1** along [101] features two 3D interpenetrating nets with a 4,3-connected tbo topology. The uranyl centers are represented as yellow polyhedron whereas the carbon atoms are shown as black sticks. The oxygen and hydrogen atoms are not drawn for clarity. Bottom: The individual 3D nets are shown in two different colors (yellow and orange) to highlight the interpenetration of the two 3D networks.

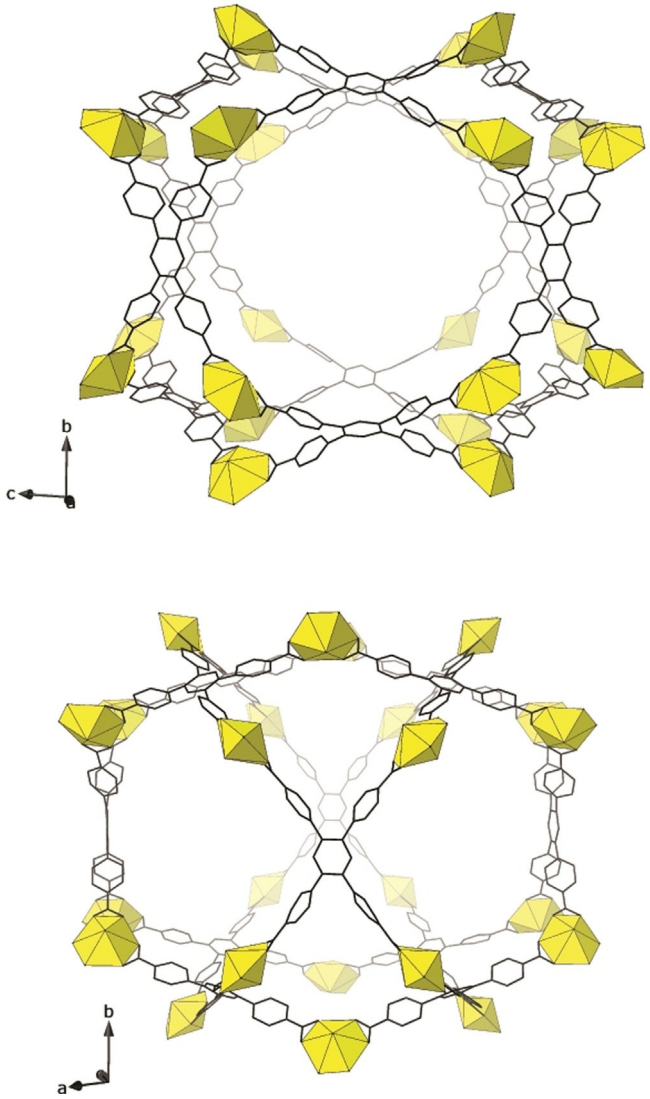

Figure 3. A single channel in **RPL-1** is shown down the [100] (**top**) and [001] (**bottom**) directions.

to roughly 8% of the material by mass. This is attributed to the decomposition of the carboxylate moieties of the TCPB ligands. A complete degradation of the framework occurs above ≈420 °C to ultimately yield U_3O_8. The thermal properties are reproducible and analyses of bulk specimens (combinations of multiple synthetic batches) exhibit analogous behavior. This level of analysis was also performed on an activated sample of **RPL-1** to demonstrate that solvent exchange and temperature treatment (up to 120 °C for 72 hours) does not have a deleterious effect upon the crystal structure. The results reveal a decrease in observed solvent mass loss, but otherwise the behavior is consistent with as synthesized samples (Figure S14). Given the excellent thermal stability of **RPL-1** and the fact that no obvious visual changes to the material occurs upon exposure to ambient air, ethanol, or water we maintain that the weak nature of the diffraction is most likely attributable to poor crystallinity, yet one cannot rule out contributions from the low density of the crystal itself.[20]

Scanning electron microscopy (SEM) images of **RPL-1** suggest the bulk material and crystals were of poor quality, perhaps polycrystalline or somewhat amorphous (Figures 4 and Figures S15–18). Several crystal morphologies were present including rods, polycrystalline particles, and large blocks. The rods may be crystalline but are small and not suitable for single crystal X-ray diffraction. The particles are much larger, but are constructed of many sub-micron crystallites. The large blocks appeared crystalline, but upon visual inspection were cracked and seemingly brittle. A focused ion beam (FIB)/SEM was used to cross-section and then image one of the block crystals. The images revealed damage within the crystals beyond the surface features (Figure 5). The presence of small crevices and non-ordered porosity indicates limited long-range crystalline ordering. Drawing conclusions as to the crystallinity or quality of single crystals from visual interpretation of SEM imaging is somewhat anecdotal, yet the assessment that the product is poorly crystalline is consistent with our difficulty in obtaining high quality single crystal and powder X-ray diffraction data.

Despite the low surface area of **RPL-1** and the pores being largely occluded by interpenetration, the material displays

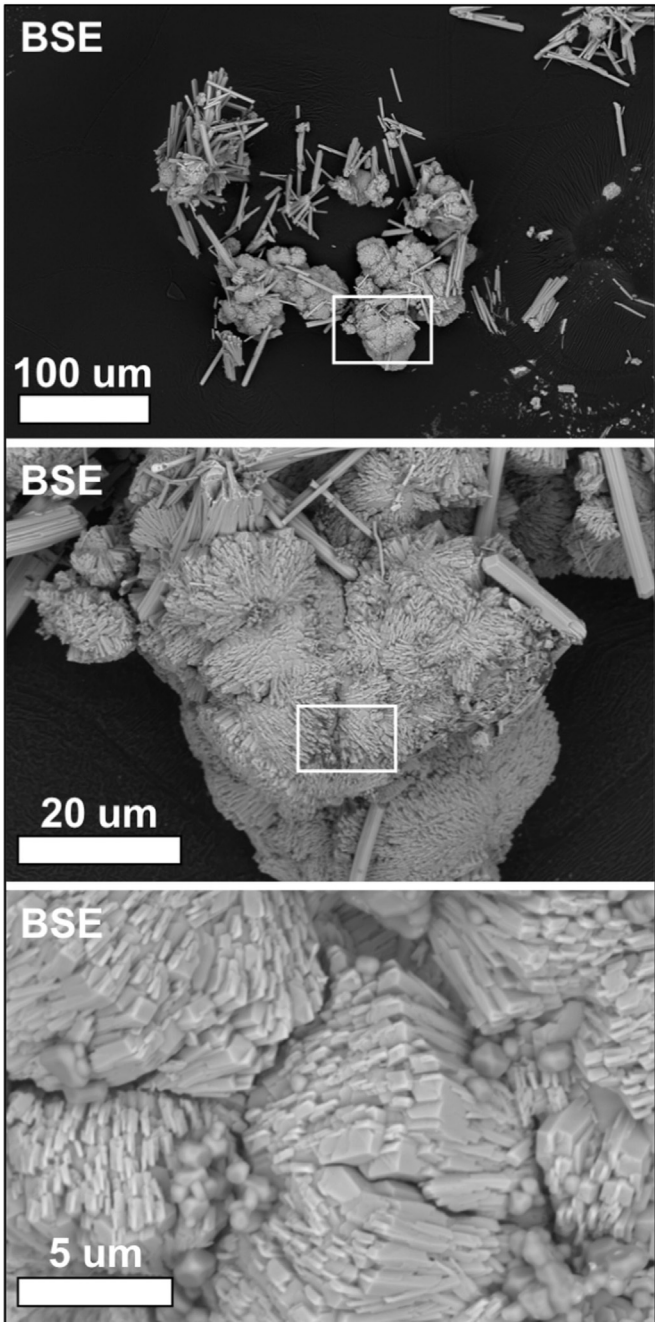

Figure 4. (Top-to-bottom) Backscattered electron images of **RPL-1** at successively higher magnifications reveal rod-like crystals and particles composed of tightly packed sub-micron sized crystallites.

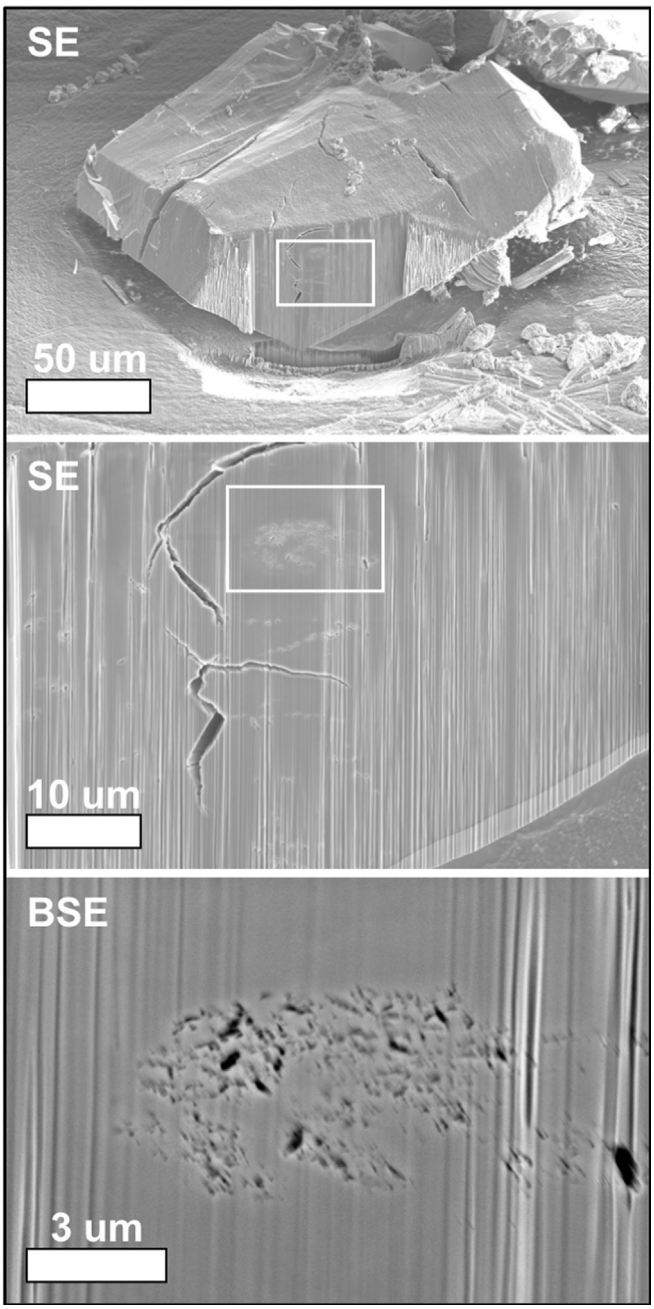

Figure 5. (Top-to-bottom) Secondary and backscattered electron images of a large block crystal of **RPL-1** at successively higher magnifications. Cross-sectioning of the crystal using a FIB reveals internal cracking, non-ordered porosity, and voids.

promise for capturing various organic dyes from aqueous media (Figure 6 and Figures S19–27 in the Supporting Information). A bulk sample of **RPL-1** (0.06 mmol) was isolated and placed directly into a 3.5 mL (0.02 mmol) solution of methyl orange (MO) dye and allowed to equilibrate. The concentration of MO was monitored in solution via absorbance spectroscopy and found to decrease by 30, 60, and 80% after intervals of 1, 24, and 72 h (Figure 6). The pale yellow-green color of **RPL-1** changed to magenta and brightened over the 72 h period. After six weeks the MOF was deep magenta in color and MO was no longer detected in solution. To assess whether **RPL-1** was selective for an anionic or cationic dye, we placed a fresh sample of **RPL-1** into a solution that contained both MO and methylene blue (MB) and monitored the solution concentration of the dyes for 72 h (Figure S20). No selectivity for one dye over the other was observed as adsorption of both occurred. This non-selective behavior is not entirely unexpected given the neutral charge of the framework. We made no attempts to explore the adsorption capacity nor kinetics governing the sequestration of MO or MB, but did probe the ability

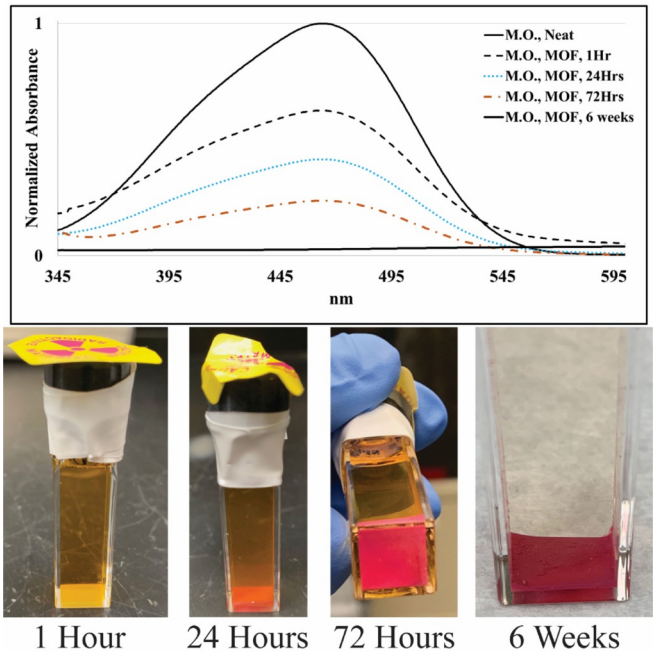

Figure 6. Top: The ability of **RPL-1** to capture MO was monitored via absorbance spectroscopy over the course of 72 h. Bottom: The color of the material changed from pale yellow-green to magenta upon adsorption of the MO dye.

to capture dyes of various size using an activated sample. This was performed to further assess the nonselective absorbance behavior without the possible interference from DMF guest species. A bulk sample of **RPL-1** was soaked in ethanol over a three day period (the EtOH was replaced every 24 h) and was thereafter isolated and heated to 110 °C for 48 h. This activated sample was placed into seven different aqueous solutions that contained rhodamine B (RB), eriochrome® black T (EB), gentian violet (GV), thionin acetate (TA), MO, MB, and a mixture of RB and MB (Figures S21–27). **RPL-1** demonstrated affinity for the capture of each dye, again with no obvious signs of selectivity, and exhibited a strong colorimetric response upon their uptake. Post adsorption, each dye can be extracted and the material recovered intact by washing with a dilute solution of ammonium hydroxide (pH 11.63). The number of possible adsorption/desorption cycles was not assessed. In summary, this material is versatile and capable of sequestering a range of charged analytes of various size and geometry, highlighting its potential use in molecular sequestration or perhaps as a platform for light-mediated processes (e.g., photocatalysis or chemical sensing).

Worthy of a final comment is that the solid-state photophysical properties of **RPL-1** were also explored on single crystals and bulk specimens. The diffuse reflectance spectrum was collected on a bulk sample and the analysis reveals strong absorbance from 300 to 500 nm (Figure S8). Absorbance in this range is typical for $O_{yl} \rightarrow U^{VI}$ charge transfer transitions,[21] yet the contribution of the TCPB ligand is clear as it absorbs strongly below 360 nm. The overlapping absorbance regions provide an opportunity to explore energy transfer between the uranyl cation and the TCPB ligands.

The luminescence properties of **RPL-1** were studied at 298 K and 77 K using single crystals and excitation wavelengths of 280, 365, and 420 nm. Excitation at 280 nm results in strong ligand-based emission between 370–405 nm (Figure 7). Excitation outside of the maximum absorbance region of the TCPB ligands at 365 and 420 nm results in ligand-based fluorescence and phosphorescence, as well as weak uranyl-based emission at ≈550 nm. Analogous measurements on bulk specimens reveal nearly identical behavior that differ only in relative intensity because of sample size (Figures S5 and S6). For example, direct excitation of the uranyl cation at 365 and 420 nm during bulk analyses reveals weak ligand-based emission and poorly resolved vibronic transitions at 523, 543, and 572 nm. Cooling the single crystals (and bulk specimens) to 77 K and utilizing the same excitation wavelengths all result in weak ligand emission and strong uranyl-based luminescence that features vibronic transitions at 502, 523, 547, 573 and 602 nm (Figure 7). The progression of the vibronic transitions is regular at ≈827 cm^{-1} and is consistent with the vibrational energy of the Raman active ν_1 symmetric stretch of the $U{=}O_{yl}$ bond, measured at 879 cm^{-1} (Figure S2). The temperature dependent luminescence behavior of **RPL-1** suggests the triplet state of the TCPB ligand (at ≈21 589 cm^{-1}) lies too close in energy to the uranyl emissive state (at ≈20 409 cm^{-1}) and provides a quenching mechanism through back energy transfer ($UO_2^{2+} \leftrightarrow$TCPB) at room temperature. The ligand triplet state energy was estimated using time-gated phosphorescence measurements at 77 K, whereas the emissive state energy of the UO_2^{2+} cation is taken as the onset of luminescence at 502 nm (Figure S7).

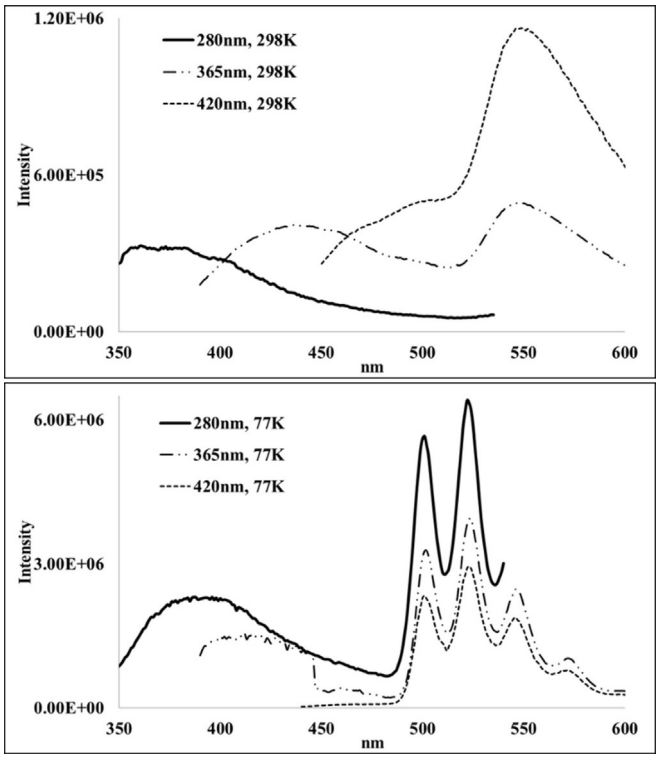

Figure 7. The emission spectra of **RPL-1** was collected on single crystals at 298 K (top) and 77 K (bottom) at various excitation wavelengths.

Lifetime spectroscopy measurements were conducted at 77 K using excitation and emission wavelengths of 420 and 521 nm, respectively (Table S2). The data was fit to a triexponential decay model and featured two lifetimes of 4.52 and 1.28×10^{-4} s (relative amplitudes of 24 and 68%, respectively) and a third, minor component of 3.36×10^{-3} s (Table S2). Decay times on the order of 10^{-4} s are consistent with the uranyl excited state,[21] whereas the minor, longer-lived component is typical of ligand-based phosphorescence. While uranyl-based emission typically exhibits monoexponential decay,[22] the two component decay observed here is attributed to the presence of multiple emissive centers owing to the four crystallographically unique uranyl sites. Finally, at 298 K the lifetime associated with the 521 nm emissive peak is triexponential and on the order of 10^{-6} to 10^{-7} s. This is wholly consistent with the presence of a temperature mediated quenching mechanism.

Conclusions

Herein we report the synthesis of a novel uranyl-containing metal–organic framework, **RPL-1**, that features 3D interpenetrated nets with 4,3-connected tbo topology. The two crystallographically unique, yet structurally analogous nets are porous (average pore size of 22.8 Å), but largely occluded by the interpenetration of the framework. **RPL-1** displayed excellent thermal and aqueous stability, and despite its interpenetrated structure the material was able to capture six different organic dye molecules from aqueous media, demonstrating no selectivity for one dye over another based on size or charge. Finally, the photophysical properties of **RPL-1** were investigated and the resulting temperature and excitation dependent behavior of the ligand-to-metal energy transfer was delineated. Energy transfer between the TCPB ligands and the uranyl metal center provided a means to largely quench the uranyl-based emission at room temperature; however, this mechanism was relaxed at 77 K and vibronically coupled uranyl emission was observed. Future work on this system will include attempts to alter the ligand geometry to disrupt interpenetration with the aim of preparing a 3D uranyl coordination network with more accessible pores and exploring the utility of this material to capture and possibly degrade organic molecules through light-mediated processes.

Acknowledgements

The research described in this manuscript was conducted under the Laboratory Directed Research and Development Program at Pacific Northwest National Laboratory, a multi-program national laboratory operated by Battelle for the U.S. Department of Energy. RGS is grateful for the support of the Linus Pauling Distinguished Postdoctoral Fellowship program. Actinide crystallographic work at LBNL was facilitated via the Heavy Element Chemistry Program, which is supported by the U.S. Department of Energy (DOE), Office of Science, Office of Basic Energy Sciences, Chemical Sciences, Geosciences, and Biosciences Division at the Lawrence Berkeley National Laboratory under Contract DE-AC02-05CH1123. All data were collected at the Advanced Light Source (ALS), which is supported by the U.S. DOE, Office of Science, Office of Basic Energy Sciences, under Contract DE-AC02-05CH11231. We thank Dr. Simon J. Teat of ALS station 12.2.1 for training and guidance throughout our single crystal X-ray diffraction studies and Professor Seth M. Cohen for facilitating gas sorption data collection. M.K. is supported by the Department of Defense (DoD) through the National Defense Science and Engineering Graduate (NDSEG) Fellowship Program and is the recipient of an Achievement Rewards for College Scientists (ARCS) Foundation Fellowship.

Conflict of interest

The authors declare no conflict of interest.

Keywords: actinide · adsorption · luminescence · metal–organic frameworks · uranium

[1] a) O. A. Ejegbavwo, C. R. Martin, O. A. Olorunfemi, G. A. Leith, R. T. Ly, A. M. Rice, E. A. Dolgopolova, M. D. Smith, S. G. Karakalos, N. Birkner, B. A. Powell, S. Pandey, R. J. Koch, S. T. Misture, H.-C. z. Loye, S. R. Phillpot, K. S. Brinkman, N. B. Shustova, *J. Am. Chem. Soc.* **2019**, *141*, 11628–11640; b) K. P. Carter, J. A. Ridenour, M. Kalaj, C. L. Cahill, *Chem. Eur. J.* **2019**, *25*, 7114–7118; c) K.-Q. Hu, Z.-W. Huang, Z.-H. Zhang, L. Mei, B.-B. Qian, J.-P. Yu, Z.-F. Chai, W.-Q. Shi, *Chem. Eur. J.* **2018**, *24*, 16766–16769; d) J. Andreo, E. Priola, G. Alberto, P. Benzi, D. Marabello, D. M. Proserpio, C. Lamberti, E. Diana, *J. Am. Chem. Soc.* **2018**, *140*, 14144–14149; e) Y. Li, Z. Yang, Y. Wang, Z. Bai, T. Zheng, X. Dai, S. Liu, D. Gui, W. Liu, M. Chen, L. Chen, J. Diwu, L. Zhu, R. Zhou, Z. Chai, T. E. Albrecht-Schmitt, S. Wang, *Nat. Commun.* **2017**, *8*, 1354; f) G. E. Gomez, J. A. Ridenour, N. M. Byrne, A. P. Shevchenko, C. L. Cahill, *Inorg. Chem.* **2019**, *58*, 7243–7254; g) E. A. Dolgopolova, A. M. Rice, N. B. Shustova, *Chem. Commun.* **2018**, *54*, 6472–6483; h) Y. Li, Z. Weng, Y. Wang, L. Chen, D. Sheng, Y. Liu, J. Diwu, Z. Chai, T. E. Albrecht-Schmitt, S. Wang, *Dalton Trans.* **2015**, *44*, 20867–20873; i) N. P. Martin, J. März, H. Feuchter, S. Duval, P. Roussel, N. Henry, A. Ikeda-Ohno, T. Loiseau, C. Volkringer, *Chem. Commun.* **2018**, *54*, 6979–6982; j) P. Li, S. Goswami, K.-i. Otake, X. Wang, Z. Chen, S. L. Hanna, O. K. Farha, *Inorg. Chem.* **2019**, *58*, 3586–3590.

[2] a) Y. Wang, X. Yin, J. Chen, Y. Wang, Z. Chai, S. Wang, *Chem. Eur. J.* **2020**, *26*, 1900–1905; b) Y. Wang, Y. Wang, X. Dai, W. Liu, X. Yin, L. Chen, F. Zhai, J. Diwu, C. Zhang, R. Zhou, Z. Chai, N. Liu, S. Wang, *Inorg. Chem.* **2019**, *58*, 2807–2812; c) Y. Wang, X. Yin, W. Liu, J. Xie, J. Chen, M. A. Silver, D. Sheng, L. Chen, J. Diwu, N. Liu, Z. Chai, T. E. Albrecht-Schmitt, S. Wang, *Angew. Chem. Int. Ed.* **2018**, *57*, 7883–7887; *Angew. Chem.* **2018**, *130*, 8009–8013.

[3] a) Z.-T. Yu, Z.-L. Liao, Y.-S. Jiang, G.-H. Li, J.-S. Chen, *Chem. Eur. J.* **2005**, *11*, 2642–2650; b) Y.-S. Jiang, Z.-T. Yu, Z.-L. Liao, G.-H. Li, J.-S. Chen, *Polyhedron* **2006**, *25*, 1359–1366; c) Z.-L. Liao, G.-D. Li, M.-H. Bi, J.-S. Chen, *Inorg. Chem.* **2008**, *47*, 4844–4853.

[4] J. Song, X. Gao, Z.-N. Wang, C.-R. Li, Q. Xu, F.-Y. Bai, Z.-F. Shi, Y.-H. Xing, *Inorg. Chem.* **2015**, *54*, 9046–9059.

[5] a) T. Loiseau, I. Mihalcea, N. Henry, C. Volkringer, *Coordin. Chem. Rev.* **2014**, *266–267*, 69–109; b) R. G. Surbella III, C. L. Cahill, *Hybrid Materials of the f-Elements Part 2: The Uranyl Cation, Vol. 48* (Eds.: J. C. Bünzli, V. K. Pecharaky), Elsevier, Amsterdam **2016**, pp. 163–285.

[6] P. C. Burns, R. C. Ewing, F. C. Hawthorne, *Can. Mineral.* **1997**, *35*, 1551–1570.

[7] P. Thuéry, J. Harrowfield, *Dalton Trans.* **2017**, *46*, 13660–13667.

[8] a) V. Mougel, L. Chatelain, J. Hermle, R. Caciuffo, E. Colineau, F. Tuna, N. Magnani, A. de Geyer, J. Pécaut, M. Mazzanti, *Angew. Chem. Int. Ed.* **2014**, *53*, 819–823; *Angew. Chem.* **2014**, *126*, 838–842; b) P. L. Arnold, *Nat. Chem.* **2012**, *4*, 967–969.

[9] H.-Y. Wu, R.-X. Wang, W. Yang, J. Chen, Z.-M. Sun, J. Li, H. Zhang, *Inorg. Chem.* **2012**, *51*, 3103–3107.

[10] Y. Wang, Z. Liu, Y. Li, Z. Bai, W. Liu, Y. Wang, X. Xu, C. Xiao, D. Sheng, J. Diwu, J. Su, Z. Chai, T. E. Albrecht-Schmitt, S. Wang, *J. Am. Chem. Soc.* **2015**, *137*, 6144 – 6147.
[11] P. Li, N. A. Vermeulen, C. D. Malliakas, D. A. Gómez-Gualdrón, A. J. Howarth, B. L. Mehdi, A. Dohnalkova, N. D. Browning, M. O'Keeffe, O. K. Farha, *Science* **2017**, *356*, 624 – 627.
[12] a) P. Li, X. Wang, K.-i. Otake, J. Lyu, S. L. Hanna, T. Islamoglu, O. K. Farha, *ACS Appl. Nano Mater.* **2019**, *2*, 2260 – 2265; b) S. E. Gilson, P. Li, J. E. S. Szymanowski, J. White, D. Ray, L. Gagliardi, O. K. Farha, P. C. Burns, *J. Am. Chem. Soc.* **2019**, *141*, 11842 – 11846; c) P. Li, N. A. Vermeulen, X. Gong, C. D. Malliakas, J. F. Stoddart, J. T. Hupp, O. K. Farha, *Angew. Chem. Int. Ed.* **2016**, *55*, 10358 – 10362; *Angew. Chem.* **2016**, *128*, 10514 – 10518; d) J. E. Warren, C. G. Perkins, K. E. Jelfs, P. Boldrin, P. A. Chater, G. J. Miller, T. D. Manning, M. E. Briggs, K. C. Stylianou, J. B. Claridge, M. J. Rosseinsky, *Angew. Chem. Int. Ed.* **2014**, *53*, 4592 – 4596; *Angew. Chem.* **2014**, *126*, 4680 – 4684; e) J. R. Karra, Y.-G. Huang, K. S. Walton, *Cryst. Growth Des.* **2013**, *13*, 1075 – 1081.
[13] N. Zhang, Y.-H. Xing, F.-Y. Bai, *Cryst. Growth Des.* **2020**, *20*, 1838 – 1848.
[14] a) X. Lian, B. Yan, *RSC Adv.* **2016**, *6*, 11570 – 11576; b) F. Hu, Z. Di, P. Lin, P. Huang, M. Wu, F. Jiang, M. Hong, *Cryst. Growth Des.* **2018**, *18*, 576 – 580; c) A. V. Desai, S. Sharma, S. K. Ghosh, *4: Metal – Organic Frameworks for Recognition and Sequestration of Toxic Anionic Pollutants* (Ed.: S. K. Ghosh), Elsevier, **2019**, pp. 95 – 140; d) Y.-J. Gao, M.-L. Feng, B. Zhang, Z.-F. Wu, Y. Song, X.-Y. Huang, *J. Mater. Chem. A* **2018**, *6*, 3967 – 3976; e) M. Feng, P. Zhang, H.-C. Zhou, V. K. Sharma, *Chemosphere* **2018**, *209*, 783 – 800.
[15] a) K. X. Wang, J. S. Chen, *Acc. Chem. Res.* **2011**, *44*, 531 – 540; b) H. D. Burrows, T. J. Kemp, *Chem. Soc. Rev.* **1974**, *3*, 139 – 165.
[16] M. Li, D. Li, M. O'Keeffe, O. M. Yaghi, *Chem. Rev.* **2014**, *114*, 1343 – 1370.
[17] L. Shao, F. Zhai, Y. Wang, G. Yue, Y. Li, M. Chu, S. Wang, *Dalton Trans.* **2019**, *48*, 1595 – 1598.
[18] S. S.-Y. Chui, S. M.-F. Lo, J. P. H. Charmant, A. G. Orpen, I. D. Williams, *Science* **1999**, *283*, 1148 – 1150.
[19] A. Spek, *Acta Crystallogr. Sect. D* **2009**, *65*, 148 – 155.
[20] S. Øien-Ødegaard, G. C. Shearer, D. S. Wragg, K. P. Lillerud, *Chem. Soc. Rev.* **2017**, *46*, 4867 – 4876.
[21] L. S. Natrajan, *Coord. Chem. Rev.* **2012**, *256*, 1583 – 1603.
[22] J. Tits, C. Walther, T. Stumpf, N. Macé, E. Wieland, *Dalton Trans.* **2015**, *44*, 966 – 976.

Manuscript received: December 22, 2019
Revised manuscript received: July 7, 2020
Accepted manuscript online: July 18, 2020
Version of record online: October 1, 2020